Results in Physics 10 (2018) 126–131

Contents lists available at ScienceDirect

Results in Physics

journal homepage: www.elsevier.com/locate/rinp

Influence of Cu and Ag doping on structure and optical properties of In_2O_3 thin film prepared by spray pyrolysis

Nasser Y. Mostafa[a,b,*], Ali Badawi[c], Sameh I. Ahmed[c,d]

[a] Chemistry Department, Faculty of Science, Taif University, P.O. Box 888, 21974 Taif, Saudi Arabia
[b] Chemistry Department, Faculty of Science, Suez Canal University, 41522 Ismailia, Egypt
[c] Physics Department, Faculty of Science, Taif University, P.O. Box 888, 21974 Taif, Saudi Arabia
[d] Physics Department, Faculty of Science, Ain Shams University, 11566 Cairo, Egypt

ARTICLE INFO

Keywords:
In_2O_3
Thin film
Spray pyrolysis
Doping
Band gap
Silver doping
Copper doping

ABSTRACT

Thin films of In_2O_3 and In_2O_3 doped with Ag^+ or Cu^{2+} were assembled by spray pyrolysis from aqueous solution at 450 °C. The microstructure analysis and optical properties were investigated using XRD, SEM, EDX and UV–Vis. spectrophotometer. XRD analysis proved that Ag-doping greatly reduces the crystallites sizes of In_2O_3 from 96 nm to 59 nm. However, Cu-doping has less pronounced effect on the crystallite sizes than that of Ag doping. The band gap energy of In_2O_3 decreases with both Cu^{2+} and Ag^+ doping. The change in lattice parameter of cubic In_2O_3 with Cu and Ag substitutions is compatible with the ionic radius of the substituted ions, i.e. Ag-substitution increases the lattice parameter and Cu-substitution decreases the lattice parameter. The calculated direct band gap of bare In_2O_3 film is 3.59 eV. Doping In_2O_3 with Cu^{2+} and Ag^+ decreases the band gap to 3.36 eV and 3.27 eV, respectively. Ag^+ substitution in place of In^{3+} ion in In_2O_3 cubic lattice causes negative strain value due to the shrinkage of the interplaner spacing of the unit cell. In contrary, replacing In^{3+} cation with Cu^{2+} cation expands interplaner distances of the crystallographic planes of In_2O_3 lattice and causes positive strain value. The present work demonstrates the capability to assemble high quality doped – In_2O_3 thin films by simple solution based spray pyrolysis.

Introduction

Solution assembled thin-films of metal oxides are promising low-cost technique for manufacture optoelectronic devices [1,2]. Generally, spin, spray and inkjet printing coatings are the most famous solution processing techniques used for deposition of metal oxides thin films [3–7]. Spray coating technique has many advantages, including; low cost and easily scalable to industrial scale. In fact, spray coating was approved in commercial production of transparent semiconductor thin films.

Indium oxide (In_2O_3) is wide band gap semiconductor metal oxide (n-type) with high electron mobility [8,9].Crystalline In_2O_3 is used many technological applications like sensors [10], liquid crystal displays [11] and solar cells [12]. Amorphous In_2O_3 thin films find wide applications flexible flat panel displays and thin-film transistors (TFTs), because of its low processing temperature; below 150 °C [2,6,13,14].

The microstructure and optoelectrical properties of In_2O_3 thin films can be tuned with controlling the type and amounts of defects [4,15], which greatly influenced by processing condition [16] as well as by foreign cation doping [10,17,18]. Insertion of dopants in In_2O_3 lattice can develop desirable optical and electrical properties [4]. Investigators [8,15,19–21], found that doping In_2O_3 with metal cations, such as Nb, Al, Sn, W, Ti, V and Mo changes have great impact on optoelectronic properties. The change in the electrical conductivity results from substitution of cations with different charges, radius and mobility. Also, lattice defect and strain which mainly produced from substitution of In^{3+} with cations of different radius, improves the charge separation [22].The band gap of In_2O_3 thin films can be tuned by doping [4,15].

The present work demonstrates the capability to assemble high quality Cu and Ag-doped In_2O_3 thin films by simple solution based spray pyrolysis.

Experimental

Spray pyrolysis processing of Ag and Cu doped In_2O_3 thin films

A home-made spray processing apparatus is used for thin films growth. The glass substrate was fixed on steel block (15 × 15 × 2 cm) containing heating elements and thermocouple for temperature control. A computer-controlled spray gun (0.3 mm nozzle diameter) was used

* Corresponding author at: Chemistry Department, Faculty of Science, Suez Canal University, 41522 Ismailia, Egypt.
E-mail address: nmost69@yahoo.com (N.Y. Mostafa).

https://doi.org/10.1016/j.rinp.2018.05.030
Received 21 April 2018; Received in revised form 16 May 2018; Accepted 16 May 2018
Available online 23 May 2018

for thin films processing. Compressed air was used as carrier gas and the flow rates were fixed at 6.5 L/min. The substrates were microscopic glass sheets with thickness 1 mm. the substrates were cleaned with ultrasonic in deionized water and alcohol. The glass substrates were cleaned in ultrasonic bath using acetone then dried with nitrogen flow. The temperature of the glass substrate was fixed at 450 °C.

Indium nitrate; $In(NO_3)_3$, silver nitrate; $AgNO_3$ and Copper(II) nitrate trihydrate; $Cu(NO_3)_2{\cdot}3H_2O$ were used to prepare the spraying solutions in deionized water as the solvent. In case of Cu and Ag-dopped In_2O_3, the amount of $AgNO_3$ and $Cu(NO_3)_2$ was fixed at M/(M + In) atomic ratios of 3. The film thickness was optimized with series of experiments at different spraying time and the thickness was measured by both weight difference and SEM measurement of cross-section. The thicknesses of the films nearly fixed in the range 300–350 nm. The substrate was sprayed for 5 s 3 times with 2 min pause time.

The XRD diffraction patterns were collected for the three film samples using a D8 ADVANCE (Bruker, USA) X-ray diffractometer with Cu Kα (λ = 1.54056 Å) operated at 40 kV and 40 mA. The diffracted intensity was measured using a LYNXEYE detector comprising 191 channels which enables good statistics for measured diffracted intensities even for thin films or minute samples. The scanning speed was 0.2°/min and the scanning angle ranged from 20° to 80° in diffraction angle. The optical properties of the thin films were investigated using UV–visible spectrophotometer (JASCO V670).

Results and discussion

XRD analysis and microstructure

Phase identification was performed for the obtained XRD patterns to define the phases comprising each film sample. The phases were identified by comparing the characteristic peaks with the JCPDS files. The cubic phase of In_2O_3 (JCPDS # 01-088-2160) with the space group $Ia\bar{3}$ was found common and dominating the composition in the three studied films. Whereas, the film doped with Cu was found to contain some weak peaks belonging to a cubic phase of Cu_2O (JCPDS # 00-034-1354) with the space group *Pn3m* and only the strongest (1 1 1) reflection of this phase can be seen as shown in Fig. 1, while the other peaks were very weak to be illustrated in the comparison of the XRD patterns.

It worth mention that, the films are characterized with a considerable degree of preferred orientation which has affected the relative intensities of the Bragg peaks. This is clearly seen especially for the (4 0 0) and its second order reflection (8 0 0) which is relatively strong in the Ag/In_2O_3 film. Moreover, the Cu_2O phase also shares this behavior and shows a certain degree of preferential orientation in the (1 1 1) plane which can be responsible for the reduction of the other peaks

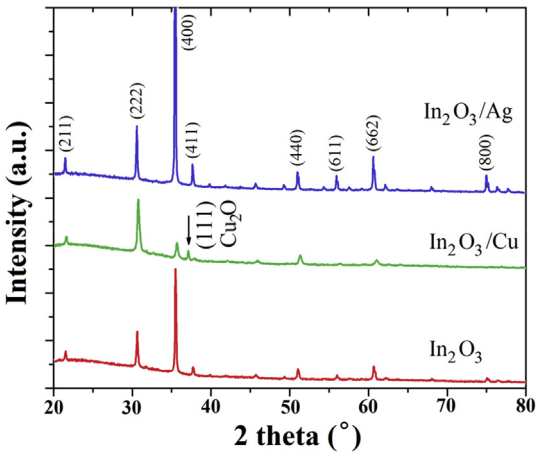

Fig. 1. Diffraction patterns of In_2O_3, Cu/In_2O_3 and Ag/In_2O_3 thin films.

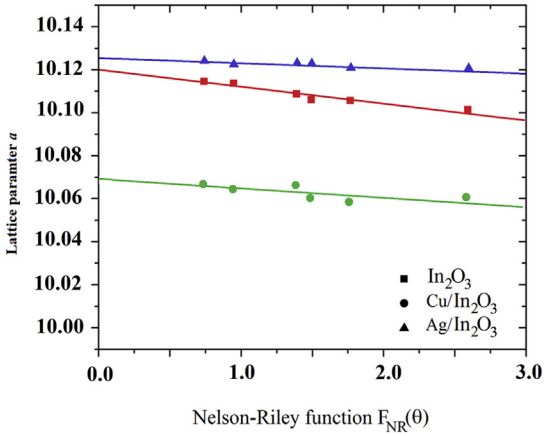

Fig. 2. Nelson-Riley plots for the samples In_2O_3 (squares), Cu/In_2O_3 (circles) and Ag/In_2O_3 (triangles), the solid lines are the best linear fits for the data.

intensities. Surely, for such cases of modified relative intensities of X-ray reflections, performing quantitative analysis becomes irrelevant. In the further analysis, attention is focused on revealing accurate lattice parameters through a least square method and on size-stain analysis to obtain reliable results. The Nelson-Riley extrapolation method [23] is used to refine accurate lattice parameters through a least-square analysis by minimizing the errors of systematic and/or random origin. For cubic crystals, like In_2O_3, each reflection can be used directly to estimate a value of the cell parameter *a*, then these value are plotted against the Nelson-Riley extrapolation function $F_{NR}(\theta)$ which can be calculated using the following relation:

$$F_{NR}(\theta) = 1/2[cos^2(\theta)/sin(\theta) + cos^2(\theta)/\theta]$$

The true value of the cell parameter is then obtained by extrapolation to $F_{NR}(\theta) = 0$ or for $\theta = 90^\circ$ as shown in Fig. 2. In other words this is given directly by the y-intercept of the above linear equations. The Nelson-Riley plots for the three thin films are shown together in Fig. 2, where the fitting lines are represented by the linear equations in Table 1. The values of the cell parameter a_o are quoted with the estimated error obtained by the propagation of the instrumental and statistical errors as well. The estimated cell parameter of bare In_2O_3 thin film is 10.119 Å, which with great agreement with literature [24]. Substitution of In ion with Ag ion increases the lattice parameter to 10.125 Å, because Ag ion has larger ionic radius than In ion. However, substitution of In ions with Cu ions decreases the lattice parameter to 10.068 Å, because Cu ion have smaller ionic radius than that of In ion.

Deviations from perfect crystals which extend infinitely in all directions and/or the perfect periodicity are always encountered in real samples, especially doped samples. Both the finite crystallite size and lattice strain are the two main properties which could be extracted from the peak width analysis. No doubt that, X-ray Line-profile analysis methods are easy and effective way to estimate the crystallite size and lattice strain [25]. In spite of the fact that, X-ray profile analysis is an average method, they still occupy an inescapable place for grain size determination, apart from imaging techniques like TEM micrographs. Williamson-Hall analysis is a straightforward and easy method wherein both the size-induced and strain-induced contributions to peak broadening are deconvoluted by plotting the peak widths versus the

Table 1
The obtained results of the Nelson-Riley extrapolation of lattice cell parameter.

Thin film	Nelson-Riley linear fit	a_0 (Å)
In_2O_3	$y = 10.11928 - 0.00741 * x$	10.1193(8)
Cu/In_2O_3	$y = 10.06813 - 0.0036 * x$	10.0681(7)
Ag/In_2O_3	$y = 10.1249 - 0.00173 * x$	10.1249(9)

diffraction angle 2θ for all present reflections [26]. In the present study, Williamson-Hall analysis is utilized to estimate crystallite size and lattice strain of pure, Cu-doped and Ag-doped In_2O_3 films. To remove the instrumental contribution, the line broadening of a standard material almost free off any sample imperfections such as corundum is firstly determined and is then considered to represent the instrumental broadening. The instrument corrected broadening β corresponding to the diffraction peaks of bare and doped In_2O_3 films was estimated using the relation:

$$\beta = \beta_{sample} - -\beta_{corundum}$$

Combination of both the Scherrer equation for the crystallite size $D = k\lambda/\beta_D cos(\theta)$ with the lattice strain equation; $\varepsilon = \beta_S/tan(\theta)$, gives the equation frequently used in Williamson-Hall analysis:

$$\beta cos(\theta) = (K\lambda/D) + 4\varepsilon\, sin(\theta)$$

The separation of size and strain contribution is achieved thanks to the different behaviors of Scherrer-equation which follows a 1/cosθ dependency and the tanθ dependence of the strain broadening. Plots of $\beta\cos(\theta)$ versus 4 $sin(\theta)$ are shown in Fig. 3 and are fitted to lines using a least square method. The linear fitting results of these plots give the straight line equations quoted in Table 2 together with the crystallite size and strain values.

The obtained negative value of the strain in the case of Ag/In_2O_3 corresponds to the shrinkage of the interplaner spacing of the cubic lattice of In_2O_3, this is in accordance with the insertion of Ag^+ cations with larger ionic radius which compresses the crystallographic planes of the In_2O_3 cubic lattice and at the same time results in the larger lattice parameter in this case as well. On the other hand, the case of Cu/In_2O_3, it has positive strain value due to the expansion of the interplaner distances of the crystallographic planes of In_2O_3 cubic lattice. This is a direct consequence of the replacement of In^{3+} cations by the smaller Cu^{2+} cations and which is confirmed by the smaller lattice parameter in this case.

Microstructure (SEM and EDX)

Fig. 4 presents all the scanning electron microscope (SEM) images of the prepared thin films and their corresponding EDX spectra. All images

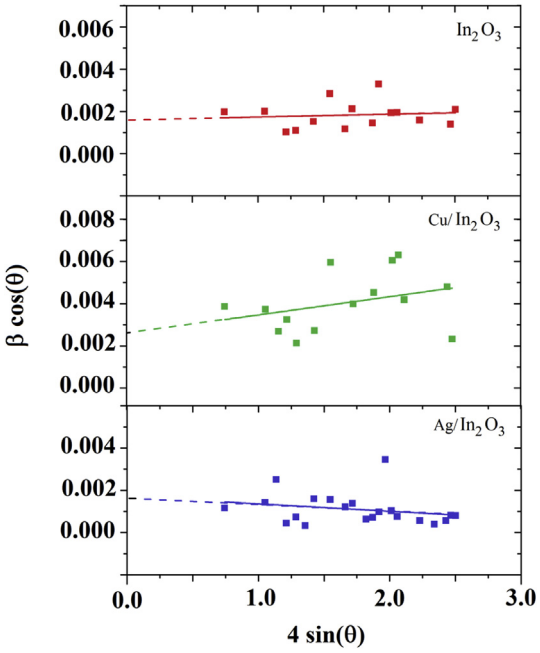

Fig. 3. Williamson-Hall plot of pure In_2O_3, Cu-doped and Ag-doped In_2O_3 thin films.

Table 2
Williamson-Hall analysis of bare In_2O_3, Cu-doped and Ag-doped In_2O_3 thin films.

Thin film	Williamson-Hall linear fit	D (nm)	ε
In_2O_3	$y = 0.0016 + 1.31551E{-}4{*}x$	96(5)	0.0002(1)
Cu/In_2O_3	$y = 0.00259 + 8.66124E{-}4{*}x$	59(3)	0.0009(7)
Ag/In_2O_3	$y = 0.00171{-}3.5255E{-}4{*}x$	90(5)	−0.0004(2)

show continuous uniform morphologies. The bare In_2O_3 thin film (Fig. 4a) shows dense layer with uniformly scattered will defined cubic crystallites. Both Ag-doped In_2O_3 (Fig. 4b) and Cu-doped In_2O_3 (Fig. 4b) thin films show of uniform more compacted layer and Ag-doped In_2O_3 has relatively smaller grains than Cu-doped In_2O_3. EDX spectra of bare In_2O_3, Ag-doped In_2O_3 and Cu-doped In_2O_3 are shown in Fig. 4d, e and f, respectively. The spectra support the incorporation of both Ag and Cu in the sprayed films.

Optical characterization

The optical properties of the prepared bare In_2O_3, Cu and Ag doped In_2O_3 thin films have been investigated using UV–visible spectrophotometer. Fig. 5 shows the transmittance (T) and reflectance (R) spectra of the prepared films in the wavelength range from 300 nm to 2000 nm. It is clearly seen that transmittance (T) of bare In_2O_3 is more than 70% in the visible spectrum region, while it is more than 60% in the same region for Cu and Ag doped In_2O_3 thin films. These novel results emphasize the proper use of these films in many related applications especially in photovoltaic applications. Moreover, at any wavelength the bare In_2O_3 film transmittance spectrum is more than that of doped ones. Also, a clear red shifts in the transmittance spectra in the doped In_2O_3 films with respect to the bare In_2O_3 film. These results are mainly attributed to the increase in the absorption spectra as will be shown later of the doped films relative to that of the bare one.

The optical energy band gap (E_g) of the prepared bare In_2O_3, Cu and Ag doped In_2O_3 thin films were deduced from the transmittance (T) spectra measurements using the Tauc equation [27–30]:

$$\alpha h\nu = A(h\nu - E_g)^n$$

where $\alpha = \frac{1}{d} ln \frac{1}{T}$ is the optical absorption coefficient [29], T is the transmittance measurements, d is film's thickness, ν is the frequency of the incident spectrum, h is Planck's constant, A in a constant, n value depends on the type of optical transition which takes values: 1/2, 3/2, 2 or 3 for direct allowed, direct forbidden, indirect allowed and indirect forbidden transitions, respectively. Since In_2O_3 is a direct band gap semiconductor, "n" value in Tauc equation equals 1/2. The values of E_g of the prepared films are estimated by plotting $(\alpha h\nu)^2$ as a function of the incident spectrum $h\nu$ and extrapolating the linear region of these curves to $(\alpha h\nu)^2 = 0$ as shown in Fig. 6. The deduced E_g values of bare In_2O_3, Cu and Ag doped In_2O_3 thin films are listed in Table 3. It is clearly seen that the estimated E_g of bare In_2O_3 film equals 3.59 eV, which is in good agreement with the published data using different preparation techniques [31,32]. This E_g value made In_2O_3 plays the role of an efficient candidate as an n-type window for solar cells applications. While when In_2O_3 is doped with Cu and Ag, a clear decrease in E_g is achieved to be 3.36 eV and 3.27 eV respectively. This E_g decrease is mainly attributed to the participation of Cu and Ag through efficient substitution of Indium (In) atoms, since the E_g of Cu_2O and Ag_2O are 2.2 eV and 1.2 eV respectively [33,34]. The substitution of In atoms with Cu and Ag atoms lowers the conduction band of the host material (In_2O_3) to more negative values. This behavior was concluded by other authors. Fan Ye et al. [34] concluded that adding fluorine to cuprous oxide leads to narrowing the energy band gap of the doped material. Our results of narrowing the energy band gap of In_2O_3 by doping it with metals as Cu and Ag will be sounded in many applications.

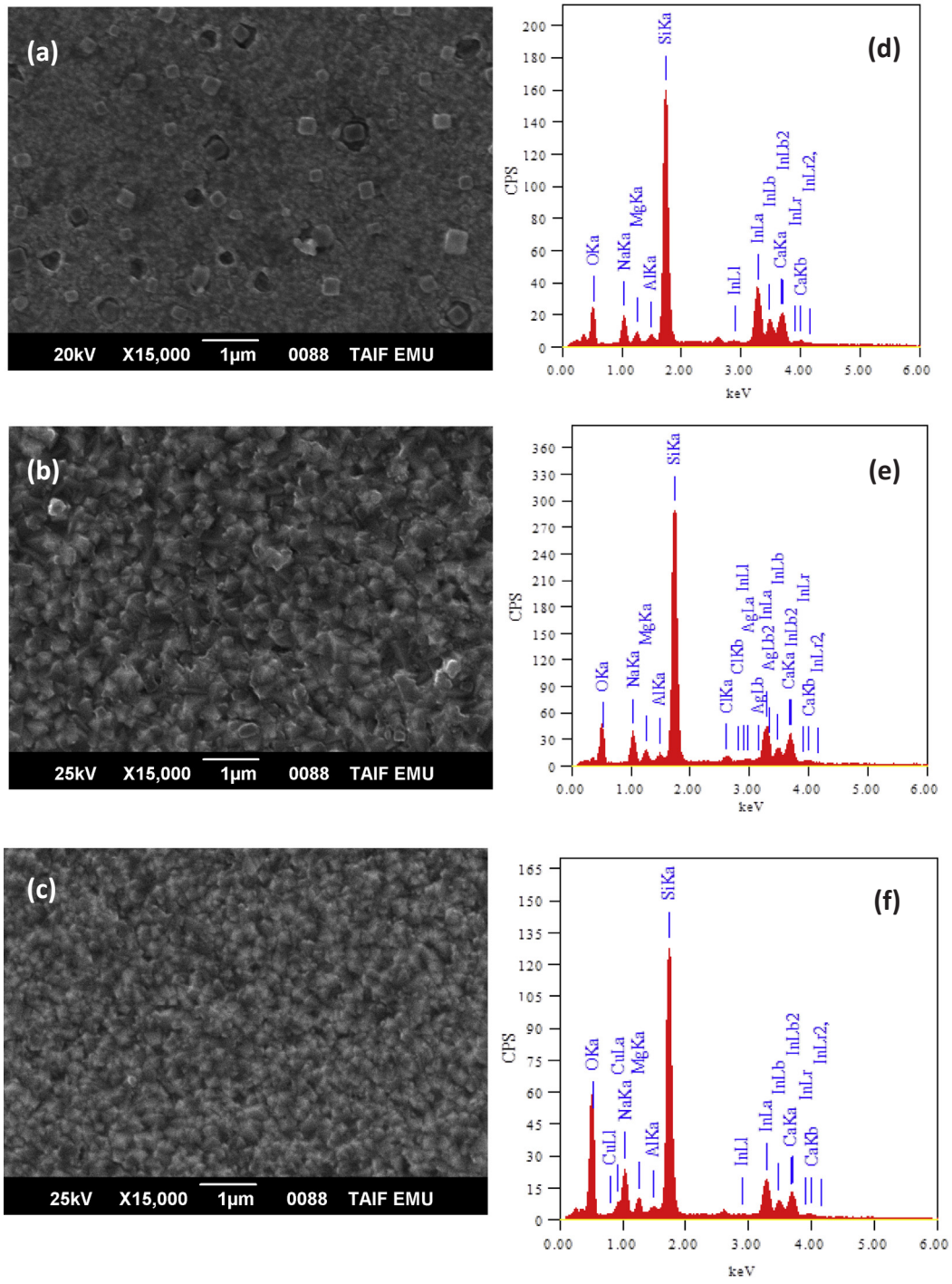

Fig. 4. SEM and EDX of different thin films; (a) and (d) In_2O_3, (b) and (e) Ag-doped In_2O_3 and (c) and (f) Cu-doped In_2O_3.

Moreover, the refractive index (n) of the prepared bare In_2O_3, Cu and Ag doped In_2O_3 thin films as a function of the incident wavelength is also studied. The refractive index of the prepared films were also deduced from the extinction coefficient (K) data and the reflectance (R) spectra measurements the wavelength range from 300 nm to 2000 nm using Fresnel formula as given [35,36]:

$$n = \left(\frac{1+R}{1-R}\right) + \left[\frac{4R}{(1-R)^2} - K^2\right]^{1/2}$$

where K (= αλ/4π) [30,37] is the extinction coefficient of the film, α is the optical absorption coefficient, R is the reflectance and λ is the incident wavelength. The refractive index (n) of the prepared bare In_2O_3, Cu and Ag doped In_2O_3 films in the wavelength range from 300 nm to 2000 nm are shown in Fig. 7. It is noticed that the refractive index (n) of any prepared film depends on the incident wavelength λ. Moreover, at almost of the wavelength range of our study (300 nm to 2000 nm), the refractive index of bare In_2O_3 film is larger than that of both Cu and Ag doped In_2O_3 films. Our results are consistent with previous studies [38,39].

Furthermore, the real (ε_r) and imaginary (ε_i) parts (called loss part) of the optical dielectric constant are also calculated using the following equations [35,38]:

$$\varepsilon_r = n^2 - k^2$$

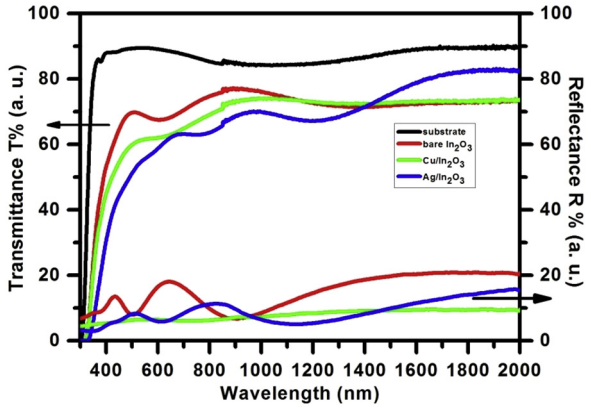

Fig. 5. The transmittance (T) and reflectance (R) spectra of bare In_2O_3, Cu and Ag doped In_2O_3 thin films.

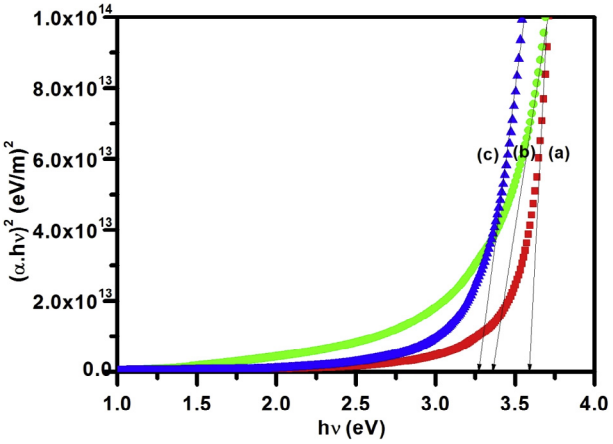

Fig. 6. $(\alpha h\nu)^2$ vs. $h\nu$ of (a) bare In_2O_3, (b) Cu-doped (c) Ag-doped In_2O_3 films respectively.

Table 3
Energy band gap of bare In_2O_3, Cu and Ag doped In_2O_3 thin films.

Thin film	Energy band gap (eV)
In_2O_3	3.59
Cu/In_2O_3	3.36
Ag/In_2O_3	3.27

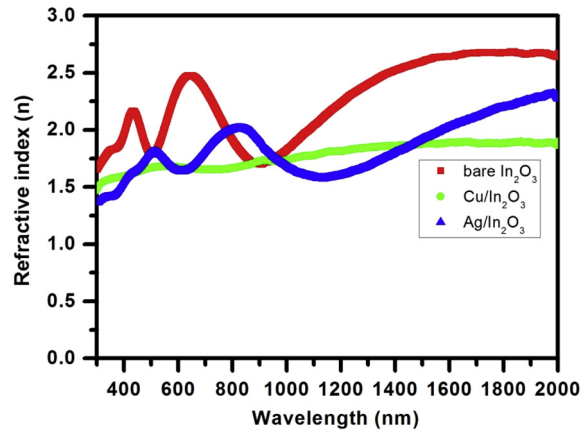

Fig. 7. The refractive index (n) of bare In_2O_3, Cu and Ag-doped In_2O_3 films versus the incident wavelength.

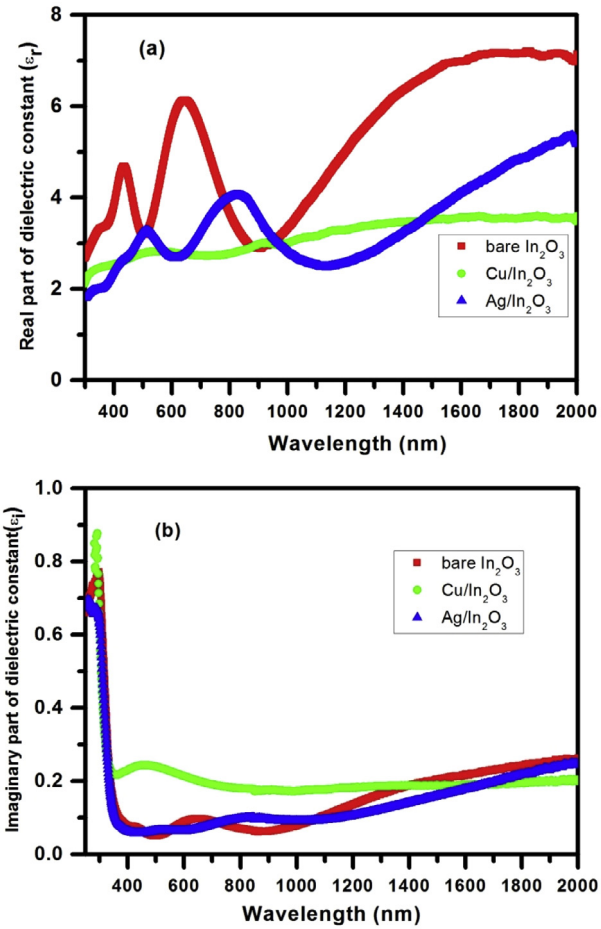

Fig. 8. (a) The real and (b) imaginary parts of the optical dielectric constant of the prepared bare In_2O_3, Cu and Ag-doped In_2O_3 films versus incident wavelength.

$$\varepsilon_i = 2nk$$

where n and K are the refractive index and the extinction coefficient respectively. Fig. 8(a) and (b) illustrates the real and imaginary parts of the optical dielectric constant of the prepared bare In_2O_3, Cu and Ag doped In_2O_3 films in the wavelength range from 300 nm to 2000 nm. The behavior of these parameters is directly related to the energy density of states within the optical band gap of the films [38,40]. It is clearly seen that the behavior of the real part of the optical dielectric constant follows the trend of the refractive index (n). While the variation of the imaginary part follows the trend of the extinction coefficient (k), which is directly related to the optical absorption coefficient (α) as discussed before.

Conclusion

In the current report, thin films of indium oxide and Cu and Ag doped indium oxide have been processed by spray pyrolysis (450 °C). XRD analysis proved that Ag doping greatly reduces the crystallites sizes of In_2O_3 from 96 nm to 59 nm. However, Cu-doping has less pronounced effect on the crystallite sizes than that of Ag-doping. The calculated direct band gap of bare In_2O_3 film equals 3.59 eV, which makes it to play the role of an efficient candidate as an n-type window for solar cells applications. Doping In_2O_3 with Cu^{2+} and Ag^{+} decreases the band gap to 3.36 eV and 3.27 eV, respectively. Ag^{+} substitution in place of In^{3+} ion in In_2O_3 cubic lattice causes negative strain value due to the shrinkage of the interplaner spacing of the unit cell. In contrary, replacing In^{3+} cation with Cu^{2+} cation expands interplaner distances

of the crystallographic planes of In_2O_3 lattice and causes positive strain value. Defects and stain in semiconductor lattice slows the rate of charge recombination in the electron transfer process [41,42]. Slow rate charge recombination is an important property needed for semiconductors used in optoelectronic devices, such as solar cells.

Acknowledgements

The authors acknowledge the financial support from Taif University – Saudi Arabia (project # 1-432-1198).

Appendix A. Supplementary data

Supplementary data associated with this article can be found, in the online version, at http://dx.doi.org/10.1016/j.rinp.2018.05.030.

References

[1] Khim D, Lin YH, Nam S, Faber H, Tetzner K, Li R, et al. Modulation-doped In_2O_3/ZnO heterojunction transistors processed from solution. Adv Mater 2017;29:1605837.
[2] Choi JW, Han SY, Nguyen MC, Nguyen AHT, Kim JY, Choi S, et al. Low-temperature solution-based In_2O_3 channel formation for thin-film transistors using a visible laser-assisted combustion process. IEEE Electron Device Lett 2017;38:1259–62.
[3] Hendi AA. Junction properties of In_2O_3:Al_2O_3 composite on p-type silicon by sol-gel method. J Sol-Gel Sci Technol 2014;72:63–6.
[4] Keriti Y, Keffous A, Dib K, Djellab S, Trari M. Photoluminescence and photocatalytic properties of Er^{3+}-doped In_2O_3 thin films prepared by sol–gel: application to Rhodamine B degradation under solar light. Res Chem Intermed 2018;44:1537–50.
[5] Khan MAM, Khan W. Thickness-dependent structural and optoelectronic properties of In_2O_3 films prepared by spray pyrolysis technique. J Electron Mater 2016;45:4453–9.
[6] Leppäniemi J, Eiroma K, Majumdar H, Alastalo A. Far-UV annealed inkjet-printed In_2O_3 semiconductor layers for thin-film transistors on a flexible polyethylene naphthalate substrate. ACS Appl Mater Interfaces 2017;9:8774–82.
[7] Lee SH, Kwack YJ, Lee JS, Choi WS. Inkjet-printed oxide TFTs with solution-processed dual semiconductors. ECS Trans 2016:127–31.
[8] Islam MA, Mou JR, Roy RC, Hossain J, Julkarnain M, Khan KA. High near-infrared transmittance, high intense orange luminescence in vanadium doped indium oxide (V: In_2O_3) thin films deposited by electron beam evaporation. Optik 2018;157:208–16.
[9] Sariket D, Shyamal S, Hajra P, Mandal H, Bera A, Maity A, et al. Temperature controlled fabrication of chemically synthesized cubic In_2O_3 crystallites for improved photoelectrochemical water oxidation. Mater Chem Phys 2017;201:7–17.
[10] Korotcenkov G, Brinzari V, Cho BK. In_2O_3- and SnO_2-based ozone sensors: design and characterization. Crit Rev Solid State Mater Sci 2017:1–50.
[11] Son KS, Kim TS, Jung JS, Ryu MK, Park KB, Yoo BW, et al. Late-news paper:4 inch QVGA AMOLED driven by the threshold voltage controlled amorphous GIZO (Ga2O3-In2O3-ZnO) TFT. In: Digest of technical papers – SID international symposium; 2008. p. 633–6.
[12] Keller J, Aijaz A, Gustavsson F, Kubart T, Stolt L, Edoff M, et al. Direct comparison of atomic layer deposition and sputtering of In_2O_3: H used as transparent conductive oxide layer in $CuIn_{1-x}Ga_xSe_2$ thin film solar cells. Sol Energy Mater Sol Cells 2016;157:757–64.
[13] Leppäniemi J, Huttunen OH, Majumdar H, Alastalo A. Flexography-printed In_2O_3 semiconductor layers for high-mobility thin-film transistors on flexible plastic substrate. Adv Mater 2015;27:7168–75.
[14] Liu A, Liu GX, Zhu HH, Xu F, Fortunato E, Martins R, et al. Fully solution-processed low-voltage aqueous In_2O_3 thin-film transistors using an ultrathin ZrOx dielectric. ACS Appl Mater Interfaces 2014;6:17364–9.
[15] Reshmi Krishnan R, Chalana SR, Suresh S, Sudheer SK, Sudarsanakumar C, Santhosh Kumar MC, et al. Effect of Nb doping on the structural, morphological, optical and electrical properties of RF magnetron sputtered In_2O_3 nanostructured films. Phys Status Solidi C 2017;14:1600095.
[16] He P, Zhai BL, Yi Y. Research of ITO transparent conductive. Appl Mech Mater 2014:1025–9.
[17] Veal BW, Eastman JA. Conduction in In_2O_3/YSZ heterostructures: complex interplay between electrons and ions, mediated by interfaces. APL Mater 2017;5:042502.
[18] Beji N, Ajili M, Turki NK. Effect of heat treatment under nitrogen atmosphere on sprayed fluorine doped In_2O_3 thin films. J Electron Mater 2016;45:3251–8.
[19] Lin HY, Ning JP, Geng F. Influence of SiO2/In2O3 film acoustical waveguide on the mode index of Ti:LiNbO3 optical waveguide in acoustooptical mode converter. In: Proceedings of SPIE – The international society for optical engineering; 2004. p. 505–8.
[20] Bayer TJM, Wachau A, Fuchs A, Deuermeier J, Klein A. Atomic layer deposition of Al_2O_3 onto Sn-doped In_2O_3: absence of self-limited adsorption during initial growth by oxygen diffusion from the substrate and band offset modification by fermi level pinning in Al_2O_3. Chem Mater 2012;24:4503–10.
[21] Kanmani C, Sivaranjani V, Balaguru N, Philominathan P. Comparison of MoO_3, In_2O_3/MoO_3 and TiO_2/MoO_3 thin films by a low-cost fabrication mechanism. Int J ChemTech Res 2014;6:1968–70.
[22] Qiao Z, Mergel D. Comparison of radio-frequency and direct-current magnetron sputtered thin In_2O_3: Sn films. Thin Solid Films 2005;484:146–53.
[23] Nelson JB, Riley DP. An experimental investigation of extrapolation methods in the derivation of accurate unit-cell dimensions of crystals. Proc Phys Soc 1945;57:160.
[24] Bedoya-Calle Á, García-Méndez M, Torres-Castro A, Shaji S, Ortiz-Méndez U. Chemical characterization of DC-sputtered In_2O_3 films with a top SnO_2 layer. J Nano Res 2015;30:86–95.
[25] Cullity BD, Stock SR. Elements of X-ray diffraction. Upper Saddle River: Prentice Hall; 2001.
[26] X-ray diffraction a practical approach. Verlag: Springer; 2014.
[27] Badawi A, Al-Hosiny N, Merazga A, Albaradi AM, Abdallah S, Talaat H. Study of the back recombination processes of PbS quantum dots sensitized solar cells. Superlattices Microstruct 2016;100:694–702.
[28] Merazga A, Al-Subai F, Albaradi AM, Badawi A, Jaber AY, Alghamdi AAB. Effect of sol-gel MgO spin-coating on the performance of TiO_2-based dye-sensitized solar cells. Mater Sci Semicond Process 2016;41:114–20.
[29] Badawi A. Photoacoustic study of alloyed $Cd_{1-x}Pb_xS$ quantum dots sensitized solar cells electrodes. J Mater Sci Mater Electron 2016;27:7899–907.
[30] Badawi A, Ahmed EM, Mostafa NY, Abdel-Wahab F, Alomairy SE. Enhancement of the optical and mechanical properties of chitosan using Fe_2O_3 nanoparticles. J Mater Sci Mater Electron 2017;28:10877–84.
[31] Thirumoorthi M, Thomas Joseph Prakash J. Structure, optical and electrical properties of indium tin oxide ultra thin films prepared by jet nebulizer spray pyrolysis technique. J Asian Ceram Soc 2016;4:124–32.
[32] Oliver B. Indium oxide—a transparent, wide-band gap semiconductor for (opto) electronic applications. Semicond Sci Technol 2015;30:024001.
[33] Xu Y, Schoonen MAA. The absolute energy positions of conduction and valence bands of selected semiconducting minerals. Am Mineral 2000;85:543–56.
[34] Ye F, Zeng J-J, Cai X-M, Su X-Q, Wang B, Wang H, et al. Doping cuprous oxide with fluorine and its band gap narrowing. J Alloy Compd 2017;721:64–9.
[35] Abd El-Raheem MM, Amin SA, Alharbi MA, Badawi AM. Structural and optical characterization of Sb-doped ZnO co-sputtered thin films. J Opt Technol 2016;83:375–84.
[36] Al-Baradi AM, Al-Shehri SF, Badawi A, Merazga A, Atta AA. A study of optical, mechanical and electrical properties of poly(methacrylic acid)/TiO_2 nanocomposite. Results Phys 2018;9:879–85.
[37] Atta AA, El-Nahass MM, Elsabawy KM, Abd El-Raheem MM, Hassanien AM, Al Huthali A, et al. Optical characteristics of transparent samarium oxide thin films deposited by the radio-frequency sputtering technique. Pramana 2016;87:72.
[38] Abdullah OG, Aziz SB, Omer KM, Salih YM. Reducing the optical band gap of polyvinyl alcohol (PVA) based nanocomposite. J Mater Sci 2015;26:5303–9.
[39] Heiba ZK, Mohamed MB, Imam NG, Mostafa NY. Optical and electrical properties of quantum composite of polyvinyl alcohol matrix with CdSe quantum dots. Colloid Polym Sci 2016;294:357–65.
[40] Caglar Y, Ilican S, Caglar M, Yakuphanoglu F. Effects of In, Al and Sn dopants on the structural and optical properties of ZnO thin films. Spectrochim Acta A Mol Biomol Spectrosc 2007;67:1113–9.
[41] Zhang Y, Zhang J, Nie M, Sun K, Li C, Yu J. Photoelectrochemical water splitting under visible light over anti-photocorrosive In_2O_3-coupling ZnO nanorod arrays photoanode. J Nanopart Res 2015;17:1–11.
[42] Chen LC, Lan WH, Lin RM, Shen HT, Chen HC. Optical properties of In_2O_3 oxidized from InN deposited by reactive magnetron sputtering. Appl Surf Sci 2006;252:8438–41.